BUNCH-END INTERPENETRATION DURING EVOLUTION TO LONGITUDINAL UNIFORMITY IN A SPACE-CHARGE-DOMINATED STORAGE RING *

T. W. Koeth, B. Beaudoin, S. Bernal, I. Haber, R. A. Kishek, P.G. O'Shea, IREAP, University of Maryland, College Park, MD, 20742

Abstract

The University of Maryland Electron Ring is a facility for study of the novel physics that occurs as intense space-charge-dominated beams that are transported over long distances. An example presented here is the role of space-charge longitudinal expansion and bunch-end interpenetration in the relaxation of a coasting bunch towards uniformly filling the ring. By comparing experiment to simplified longitudinal simulations the relaxation process is shown to be largely independent of details of the transverse dynamics. However, to get detailed agreement it was found necessary to include the consequences of transverse current loss. Since the AC coupled diagnostics lose information on any DC current loss, a novel beam knockout technique was developed to recover this information.

INTRODUCTION

Space charge can strongly influence both the transverse and longitudinal evolution of an intense particle beam. Because the longitudinal dynamics evolve slowly compared to transverse dynamics, the study of the longitudinal regime is relatively unexplored. Additionally, long transport lengths are necessary to systematically explore longitudinal effects.

The ability to access the longitudinal space charge effects was a motivation for the construction of the University of Maryland Electron Ring (UMER) [1]. The UMER group has recently celebrated the transport of an intense, 10 keV electron beam for a distance in excess of 11 km [2]. To improve our investigation, it is critical to identify the beam loss and its mechanisms in UMER.

A notable characteristic of a long uniform injected beam in UMER is the space-charge-induced bunch-end erosion and longitudinal expansion that occurs in the absence of longitudinal focusing [3,4]. The expansion continues until the bunches interpenetrate, eventually leading to a uniform filling of the ring which is a direct current (DC) beam. The UMER diagnostics, such as the beam position monitors and the wall current monitor, are AC coupled, thus the accumulated DC component of the circulating beam is undetected and appears as beam loss.

In this paper we present an analytical description of the longitudinal dynamics to explain the general observed behaviour, followed by a summary of experimentally observed features. We describe axisymmetric simulations that explain these features and their underlying phenomena, and how our simple two-dimensional simulations have predicted observed longitudinal phenomena as well as how our two-dimensional simulations accurately reproduce the observed experimental measurements.

We also describe a new beam single-pulse knock-out measurement technique employed to reconstruct the DC component of the circulating beam current absent from the AC diagnostics. The measured DC component is added to the AC beam structure to recreate the complete temporal beam profile. These measurements are in turn used to refine our simulations by accounting for actual beam loss.

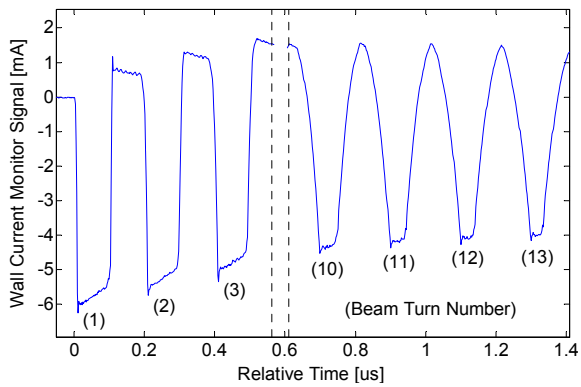

Fig. 1: Beam current as a function of time from the wall current monitor, for a 100 ns, 6 mA-peak UMER electron beam. Each pulse represents one turn. Turns 4 through 9 are omitted for clarity, the discontinuity indicated by the vertical dotted lines. The long time scale drift is an artifact of the wall current monitor.

MULTI-TURN BEAM CURRENT

Typical UMER operating conditions inject a 100 ns 10 keV electron bunch into the ring. Since the circulation time for a 10 keV electron is nominally 197 ns, the UMER ring is initially ~ 50% populated with beam. The UMER gun employs a grid distanced 0.15 mm from the cathode to switch the beam current and generate the initial beam pulse. A rotatable aperture plate located downstream of the anode grid selects the beam current. In the operation discussed here, the beam current is apertured to 6 mA from the approximately 100 mA available. Once the beam is injected into the ring, the dipole at the end of the injection line is switched off so as to permit recirculation. The transverse beam position is measured by sixteen beam position monitors (BPM) and a resistive wall current monitor is used to measure the beam current profile.

*Work supported by US Dept. of Energy Offices of High Energy Physics and Fusion Energy Sciences, and by the Office of Naval Research and the Joint Technology Office.

An illustration of the Wall Current monitor signal is plotted in Fig. 1. Turn numbers are annotated in parenthesis with turns 4 through 9 have been truncated. From this trace, a comparison can be made between the relatively sharp time profile of the head and tail of the injected pulse (turn 1) and subsequent turns. As the beam coasts, the head of the circulating bunch is accelerated, primarily by space charge, while the tail is similarly decelerated. The beam end erosion is quickly pronounced in the 2nd and 3rd turns. The tail of the 10th bunch can be seen 'meeting' the head of the 11th bunch. The head and tail then interpenetrate, ultimately leading to uniform filling of the ring with a DC beam. This is first seen at the 7 μs time stamp in Fig. 2 where the AC signal first drops to a minimum. This is followed by a resurrection of a small amplitude AC signal indicating a re-bunching. The rebunching shows a 180° phase shift after passing through the minimum, demonstrating that the peak density eventually occurs in the void between the initial beam pulses. After the 14 μs, the Wall Current monitor signal is zero.

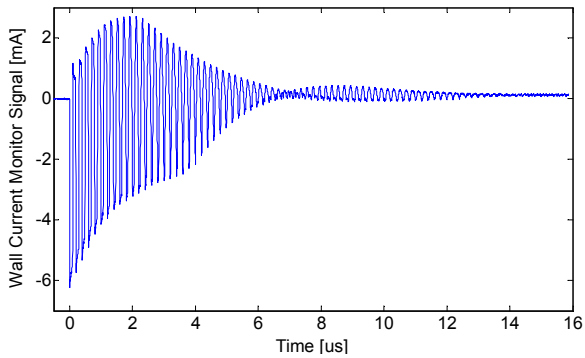

Fig. 2: The circulating 6 mA UMER electron beam current. The first minimum AC signal occurs near 7 μs in this trace, and it is followed by a resurrected AC signal indicating partial beam rebunching. Note that no AC beam structure is observed beyond 14μs.

Because the observed beam loss rate exceeds the transverse loss expected, and because the observed resurrection in the AC beam component is not easily explained by the transverse dynamics, the observed behavior, as will be discussed below, has been attributed to the longitudinal dynamics, including the accumulation of DC beam.

ANALYTICAL DESCRIPTION

The beam transport in UMER employs 36 alternating-gradient magnet cells along with one bending dipole per cell and additional vertical steering correctors to propagate a single 100 ns bunch that is injected to fill half the ring [5]. Because of the alternating-gradient focusing and the ring geometry, the beam dynamics is inherently three-dimensional. Since the space-charge intensity in UMER is significantly higher than typical rings, the beam is subject to a rich sea of possible resonances, many of which occur only because of the intense space charge.

Despite the inherent complexity of the transverse beam dynamics in UMER, a simple longitudinal model has proved to be highly useful in understanding the longitudinal dynamics. This is largely due to the separation between the relatively long timescale for the evolution of the longitudinal dynamics, which is slow compared with the traversal time of the magnet cell and the rapid transverse evolution that generally occurs on the scale of a few magnet periods.

Both the bunch length and the length scale for longitudinal variations are longer than the pipe radius. In this regime, we can use the conventional approximation for the longitudinal fields in the beam frame [1].

$$E_z(r) = \frac{-e}{4\pi\varepsilon_0} g \frac{\partial \lambda}{\partial z}. \quad \textbf{(1)}$$

Here, e is the electron charge, λ the line charge density and

$$g = 2\ln(b/a) \quad \textbf{(2)}$$

is a geometry factor, where b is the pipe radius and a the beam radius. Note however that, as will be discussed below, the geometry factor can change in the later stages of the beam evolution. Because of the accelerative cooling in the gun region, it is possible to neglect the longitudinal pressure term compared with the space charge fields and to use the cold fluid equations, along with the above model for the longitudinal fields, to derive the characteristics of the longitudinal waves supported on the bunch. These waves propagate at a velocity given by:

$$c_s^2 = g \frac{e}{4\pi\varepsilon_0 m} \lambda \quad \textbf{(3)}$$

where m is the electron mass.

In the case of an initial uniform bunch with short rise and fall times at the ends, the ends ablate due to space charge at a velocity of $2c_s$ in the beam frame. In addition, a rarefaction wave propagates into the bunch at c_s. Since UMER is a ring, the ablating front and back ends of the beam eventually intersect. At the minimum in density in the region of intersection, the longitudinal self-electric field, which is proportional to the derivative of the line density, will be zero. The two ends are therefore free to interpenetrate.

According to the prediction of this simple model, the process of interpenetration will continue until the beam reaches a DC current filling the entire ring.

LOSSLESS AXISYMMETRIC SIMULATIONS

Because the transverse evolution of the UMER beam generally occurs more rapidly than the longitudinal dynamics, it is thereby generally possible to average over the transverse variation when calculating the longitudinal

evolution. Thus it is not necessary to follow the variation in beam cross section during the traversal of an alternating gradient period. It is adequate to replace this rapid variation by an average circular cross section. In this spirit, even though the beam dynamics are inherently three-dimensional, an *r-z* approximation was employed to study the longitudinal dynamics. Axisymmetric simulations were performed using the axisymmetric module in the WARP [6] particle-in-cell code, to compare with measured current waveforms.

The simulations were performed in a frame moving with the beam with periodic boundary conditions in the axial direction applied at the 11 meter ring circumference. A major advantage of the axisymmetric model, which also employs an applied *z*-independent radial focusing force, is that merely 100 time-steps per ring period were found adequate to advance the dynamical system. Because simulations of a long bunch with longitudinal thermal velocity somewhat less than the sound speed can be subject to a longitudinal grid instability, approximately 10^7 simulation particles were employed to reduce the excitation of this instability by statistical fluctuations in the line density. A 256 cell mesh in *z* and 64 in *r* was employed. The large longitudinal mesh size was also chosen to reduce the longitudinal instability growth. To further reduce instability growth, longitudinal smoothing using a 0.25, 0.5, 0.25 stencil was applied to the potential three times per time step in the longitudinal direction. For the initial simulations, the injected matched beam radius, whose value is subject to some uncertainty, was adjusted from the nominal 3.19 mm to 4 mm such that the first DC instance, as seen at ~8 μs in Fig. 2, coincided with the measurement. The equilibrium beam radius affects c_s through the geometry factor *g*, as defined earlier, and therefore the ablation velocity of the bunch ends.

A difference between the simulation and experiment is in the long time behavior after the rebunching. This appears to be due to actual transverse beam loss in the experiment and will be discussed below. Primary among these is that the *rz* geometry employed in the simulations lacks any of the primary mechanisms for transverse current loss that are likely to be significant in the experiment. For example, as the beam particles are blown off from the bunch ends, their energies differ significantly from the nominal beam energy, which may exceed the longitudinal acceptance of the ring.

Because information on how much of beam exits the ring transversely is lost in the AC coupled diagnostics, it is difficult to estimate the relative significance of the two effects. It is therefore important to understand the degree of transverse beam loss. The knockout diagnostic discussed in the next section is motivated by this need.

MEASUREMENTS

UMER's circulating beam current is measured by a wall current monitor. The monitor is formed by an interruption of the beam pipe continuity which diverts the image current through a ferrite loaded transformer. The voltage that develops across the beam pipe gap is measured by a digitizing oscilloscope. Because of the inductive properties, the measured beam signal is convoluted with the transient response of the detector. A Cadence-PSpice model of the wall current monitor is used to compare the simulated beam current profiles with measured data. Each simulation current profile is run through the wall current monitor circuit mode, recreating the transient effect, enabling a direct comparison between the measurement trace and the simulations.

We have developed a "knock-out" technique to restore lost information of the DC component while still utilizing the existing AC coupled diagnostics. Measurements with this technique have isolated beam loss from DC buildup, indicating significant a DC beam component during the beam recirculation lifetime [6].

In the knock-out technique, a longitudinal section of the circulating beam is ejected from the ring by application of a large amplitude (1.2kV), short (50 ns) transverse voltage pulse applied between the horizontal plates of a beam position monitor. The pulse has sufficient amplitude to transversely drive a longitudinal portion of the beam into the beam pipe in less than one revolution, creating a longitudinal void or notch in the circulating DC beam. This restores a time varying structure to the circulating beam. The restored AC signal comes at the cost of beam loss, necessarily making this a partially destructive diagnostic. Provided that the knocked out portion of the beam is completely removed, the immediate restored peak-to-peak AC signal is a measure of the instantaneous beam current by reestablishing a zero-baseline for the signal.

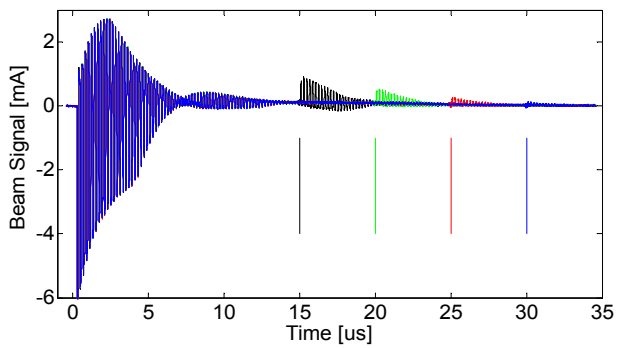

Fig. 3: Demonstration of restored AC signal from application of knock-out pulse at several different times during the beam lifetime (black: 15μs, green: 20μs, red: 25μs, and blue: 30μs). The initial peak response yields the instantaneous DC current.

There are three characteristic phases in the beam's longitudinal evolution. The first phase is the time from injection to the instant when the head meets the tail after interpenetration. The second phase in the beam's lifetime is the combined behavior of AC and DC structure. Finally, the third region is identified as the portion of the beam that has become completely DC without any detectable AC component. These phases are important in interpreting the knockout experiment. The knock-out pulse firing time in the first and last phases is straightforward. In Phase I, firing the knockout pulse in

between subsequent beam passes, as expected, has no impact on the circulating beam and confirms the lack of a beam presence.

During the third phase, when then line charge density becomes uniform, the time of the knock-out pulse firing can be arbitrary. However, during Phase II, care needs to be taken to fire the knock-out pulse during the minimum of the AC signal. The difference between the minimum of the AC signal and the resulting knocked-out Minimum is the DC pedestal. Only at this point will a difference measurement yield the DC offset. Firing the knock-out pulse at any other time during the phase would require a more sophisticated analysis of the signal, incorporating a turn-by-turn integration.

The DC beam accumulation and loss profile can be inferred by incrementally performing the knock-out over the beam life time. So far this technique has been applied to UMER's 6 mA beam; examples of four different knock-out pulses are shown in Fig. 3. Since the knock-out pulse drastically modifies the remaining beam, and because the pulser apparatus is a single shot device requiring recovery time, there can only be one knock-out pulse per beam injection. Fig. 3 displays four different beam injections, each with a different knock-out pulse firing time, in each case an instantaneous AC response is noted, the amplitude of which decreases with beam lifetime.

A complete beam loss profile has been generated for the 6 mA beam from 720 knock-out pulses nominally spaced in 50 ns increments. Once the DC portion of the beam is determined, it can be added to the AC profile to determine the overall beam profile. Integrating the true beam profile per revolution yields the average beam current, which is shown in Fig. 4. As is seen in Fig. 4, after the 6th revolution, a constant loss rate is observed until the first occurrence of the minimum AC component, (~8μs) after which the beam loss rate decreases. The reduced loss rate is also linear and continues unchanged until the UMER magnet cycle terminates 35 μs after injection. Fig. 4 shows the knock out results only to 20 μs.

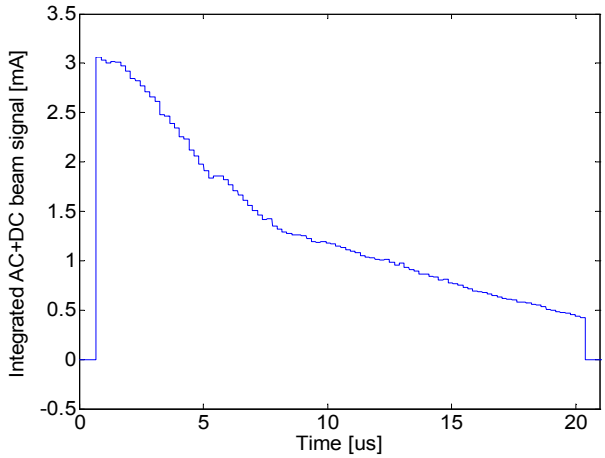

Fig. 4: The reconstructed average UMER beam current (averaged once per turn). A linear beam loss is noted after the 6th turn, the loss rate substantially decreases near 8 μs, the point of the first minimum AC signal.

LOSSY SIMULATIONS

Guided by experiment, WARP simulations were performed in which the particle weights were adjusted to match the measured beam-loss profile; this was to account for the evolution of space charge effects. A bi-linear loss mechanism was imposed on the aforementioned lossless axisymmetric simulations by linearly reducing the macro particle charge after the 1.7 μs time stamp. The first loss rate was 0.276 mA/μs until 7.8 μs, at which point the loss rate was reduced to 0.071 mA/μs which continued until the simulation's end at 20 μs. Excellent agreement was found, as seen in Fig. 5, between the measurement and simulation by adjusting several simulation parameters, including the beam radius.

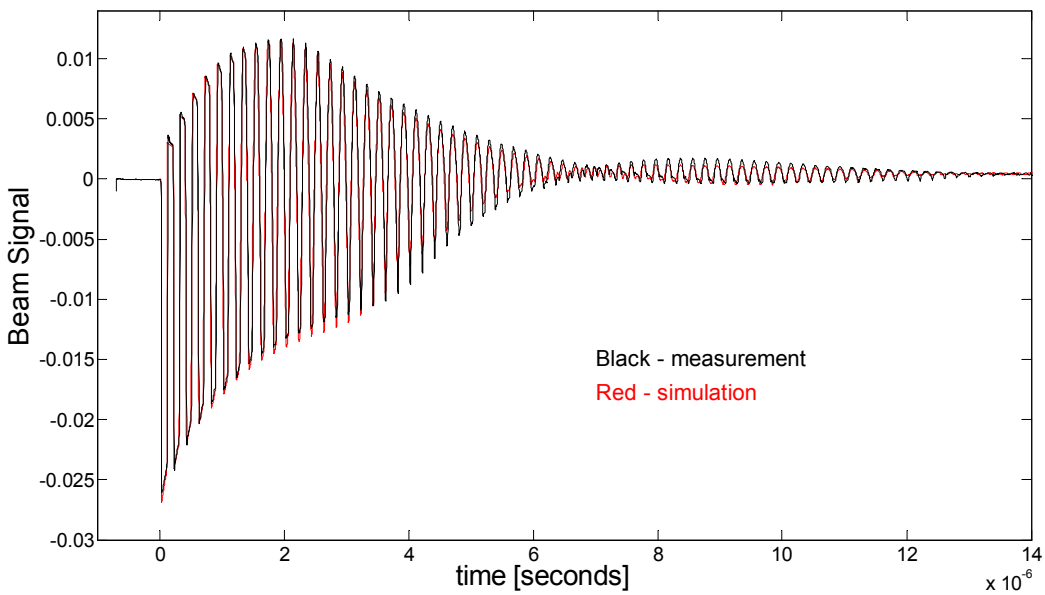

Fig. 5: Excellent agreement is seen in the comparison of 6 mA wall current monitor signal with a 'lossy' simulation current profile applied to the wall current monitor equivalent circuit model.

The first minimum AC signal location (8 μs) in simulation was found to coincide with the measurement for the known beam radius of 3.19 mm.

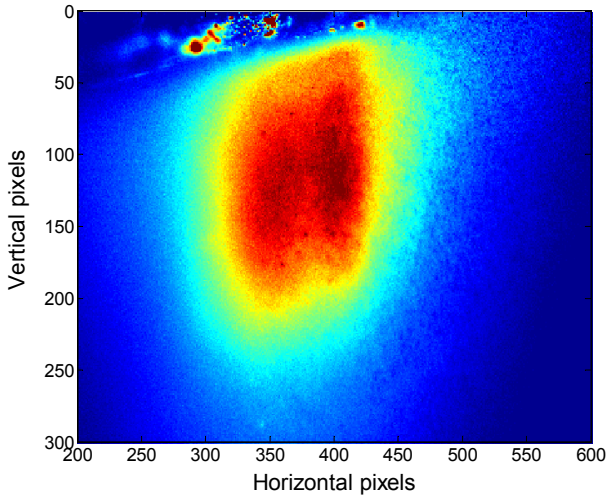

Fig. 6: Simulated longitudinal phase space plot at approximately 8 ms. The beam head and tail have overlapped three times.

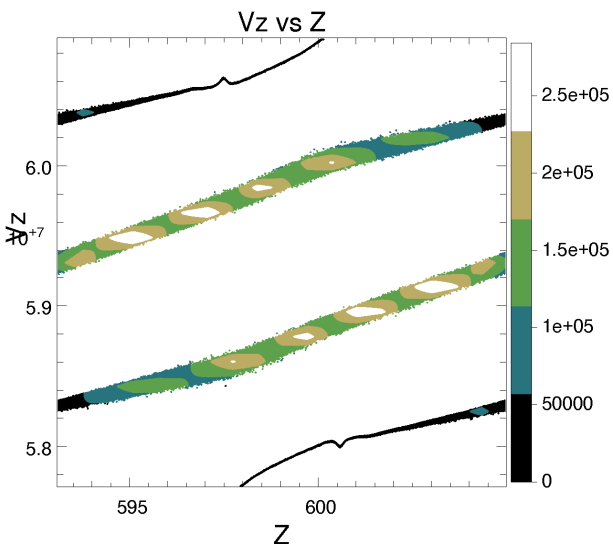

Fig. 7: Phase space plot from simulation at approximately 8 μs, coinciding with the first DC. The beam head and tail have overlapped three times.

INTERPENETRATION CONFIRMATION

A UMER Beam Position Monitor diagnostic chamber was reconfigured to house a fast acting phosphor which was positioned below and off-axis of the beam. Care was taken to the bring phosphor screen as close as possible to the beam without causing interception of the circulating beam. The HV knock-out pulser was stationed four lattice periods upstream, corresponding to ¾ of a betatron period for the 6 mA beam. The pulser was connected to the vertical pair of BPM plates. The deflection pulse amplitude was adjusted to excite a large vertical betatron motion, but without beam loss, for a short section (~10 ns) of the beam. After executing ¾ of a betatron period, the vertical excursion of the deflected beam slice was sufficiently below the orbit to fully impinge on the phosphor screen, as shown in Fig. 6. A gated PIMAX II camera, synchronized to the deflector pulse, imaged the 10 ns transverse slice; images were taken throughout the beam life time.

At approximately 8 μs, corresponding to the first DC point, two distinct coincidental beams were observed, confirming beam interpenetration. They are shown in Fig. 6. The longitudinal phase space from simulation at that instance explains why the two distinct beam energies may be seen. The full extent of the horizontal axis of Fig. 7 is the UMER circumference, again, 197 ns. It then is seen that a 10 ns slice of beam contains several discrete energies. Both dispersion and different betatron phases contribute to the two beam's transverse position. As the 10 ns gate is swept through the 197 ns circulation time, each beam is seen to develop and disappear independently. Fig. 6 shows them at the instance of equal prominence. In the case of the 6 mA beam, the discrete beams have not been discernable in the turns much beyond the 8 μs point.

Future investigations will extend to higher current beams, and will utilize the combination of the knock-out technique and transverse viewing to further explore space charge effects.

CONCLUSIONS

Coasting space-charge dominated beams have been observed to longitudinally expand to the point of head-tail interpenetration. This continues for several complete overlaps leading to the formation of a circulating DC beam while maintaining discrete transverse beam profiles. The UMER group has developed a technique to detect the DC beam component utilizing existing AC coupled diagnostics. The resulting beam profile has guided lossy simulations, which in turn have found excellent agreement with observation. These simulations will be instructive in diagnosing the beam loss mechanisms.

REFERENCES

[1] M. Reiser, *Theory and Design of Charged Particle Beams* 2nd Ed. Wiley-VCH, 2008, Ch 7.4
[2] B. Beaudoin, I. Haber, R. A. Kishek, et al, Physics of Plasmas, 18, 013104 (2011)
[3] R. Kishek, unpublished simulation result (1998); in UMER Technical Note UMER-08-0724-RAK
[4] S. Bernal et al. "Operational Studies of the 10 keV Electron Storage Ring UMER", AAC'2008 2009.
[5] A. Faltens, E.P.Lee, and S. S. Rosenblum, J. Appl. Physics **61** (12), 5219, 15 June 1987
[6] J.-L. Vay, P. Colella, J. W. Kwan, et al, Physics of Plasmas, 11, 2928 (2004)
[7] T.W. Koeth, B. Beaudoin, S. Bernal, I. Haber, R.A. Kishek, M. Reiser, P.G. O'Shea, Advanced Accelerator Concepts Workshop, 2010, pp 608-61